Automated in-situ determination of buildings' global thermo-physical characteristics and air change rates through inverse modelling of smart meter and air temperature data

Rasooli, Arash; Itard, Laure

DOI
10.1016/j.enbuild.2020.110484

Publication date
2020

Document Version
Final published version

Published in
Energy and Buildings

Energy & Buildings 229 (2020) 110484

Contents lists available at ScienceDirect

Energy & Buildings

journal homepage: www.elsevier.com/locate/enb

Automated in-situ determination of buildings' global thermo-physical characteristics and air change rates through inverse modelling of smart meter and air temperature data

Arash Rasooli *, Laure Itard

Building Energy Epidemiology, Faculty of Architecture and Built Environment, Delft University of Technology, Julianalaan 134, 2628 BL Delft, the Netherlands

ARTICLE INFO

Article history:
Received 16 April 2020
Revised 30 August 2020
Accepted 13 September 2020
Available online 18 September 2020

Keywords:
Inverse modelling
Heat loss coefficient
Smart meter
Air change rate

ABSTRACT

The advancement of smart metering and sensor technologies has opened the door to performing extensive in-situ measurements in buildings and a tendency to carry-out detailed energy and indoor climate monitoring, leading to the availability of the so-called "on-board monitoring data". The data obtained through these measurements is of high value as it can be used for identification of parameters determining health, thermal comfort, and energy use. In this article, an occupied dwelling has been inspected and monitored for one year and the in-situ measurement and meteorological data are combined to feed a physic-based energy model. For the first time, the detailed data cleaning and filtering techniques are explained to give insight for future similar studies. The data is fed to a 1st – order circuit RC model, equivalent to the building's thermal model. Next, using Genetic Algorithm in a stated optimization problem, Inverse Modelling has been applied to identify four main global thermo-physical characteristics of the building, with a special attention to the heat loss coefficient. The results are compared by analysing three feed data properties: granularity level, period length, and time period, resulting the best fit in the coldest periods. The outcomes have shown the importance of these data properties by revealing differences in the heat loss coefficient in different periods and the weakening of the heat capacitance effect when feeding the model with low granularity level data. The daily values of the heat loss coefficient are then applied in combination with construction data to determine the daily averages of hourly air change rates. Finally, the method has been evaluated in terms of accuracy and precision and the air change rates have been validated using CO_2 concentration and wind velocity. Using this method, it is possible to determine buildings' main global thermo-physical characteristics as well as the cold periods' airborne heat losses.

1. Introduction

Determination of buildings' thermo-physical characteristics is a necessary step in the assessment of buildings' thermal behavior which results in an accurate estimation of building's energy saving potential. Along the same line, numerous studies (presented in 1.1) have been dedicated to determine these characteristics using a whole range of completely different approaches. Of the most important thermo-physical characteristics, the thermal transmittance of the building envelope and the air tightness can be named. A large category of conventional methods involves direct measurement of these parameters using specific instrumentation. For instance, ISO 9869 [1] prescribes a standard method for determination of the thermal resistance and thermal transmittance of façades, using a heat flux meter and a set of two thermocouples installed on the two sides of the wall. Similarly, ISO 9972 [2] prescribes a fan-pressurization method to determine the permeability of the building, the results of which can be used for estimation of air infiltration rate. These specific methods generally require specialists, specific equipment, intrusion, investment, and long periods of measurement. For instance, following the measurement and data analysis procedure prescribed by the standard ISO 9869's Average Method [1], it can take more than a month of measurements to estimate only the thermal transmittance of a single wall [3]. Accordingly, many pieces of research have been conducted to analyze the results of these tests in alternative ways to obtain the properties quicker and more reliably [4–6]. Amongst the various methods of data analysis, inverse modelling has been widely researched. Opposite to forward modelling [7], where the inputs of a known system are fed to generate its outputs, in an

* Corresponding author.
E-mail addresses: A.Rasooli@tudelft.nl (A. Rasooli), L.C.M.Itard@tudelft.nl (L. Itard).

https://doi.org/10.1016/j.enbuild.2020.110484
0378-7788/

Nomenclature

Symbols

C	electric capacitance (F)
C_{eq}	equivalent global thermal capacitance ($Jkg^{-1}K^{-1}$)
I	electric current
k	thermal conductivity ($Wm^{-1}K^{-1}$)
l	wall thickness (m)
n	maximum number of data points fed to the model
P	global solar irradiance (Wm^{-2})
$\dot{Q}$	heat flow (W)
R	electric resistance (Ω)
R_{eq}	equitant global thermal resistance (m^2KW^{-1})
R_{eq}^{-1}	heat loss coefficient (WK^{-1})
R_c	conductive thermal resistance (m^2KW^{-1})
R^2	coefficient of determination
S_0	1solar radiation fraction parameter
S_1	constant parameter
T	temperature (K)
t	time (s)
U	thermal transmittance ($Wm^{-2}K^{-1}$)
u	model input
V	electric voltage (Volt)
$\forall$	volume (m^3)
$\dot{\forall}$	air volume flow rate (m^3s^{-1})

Superscripts

∞	associated with air medium
ac	actual
H	horizontal
th	theoretical
V	vertical
SI	interior surface
SO	exterior surface

Abbreviations

ACH	Air change per hour (h^{-1})
B1	Bedroom 1
B2	Bedroom 2
DHW	Domestic Hot Water
K	Kitchen
LR	Livingroom
RH	Relative humidity
SH	Space Heating

Indices

eq	equivalent
f	floor
gen	generation
gl	glazing (whole window)
H	heating provided for the SH
H/C	heating and cooling demand
h	associated with horizontal surface
in	associated with indoor side
n	n^{th} data point
out	associated with outdoor side
sol	solar radiation
v	associated with vertical surface
w	wall

Greek letters

α	convective heat transfer coefficient ($Wm^{-2}K^{-1}$)
Δ	difference
ρ	density (kgm^{-3})
θ	model parameter vector
η	efficiency of the heating system
μ	model output
$\mathcal{O}$	'linearization error

inverse modelling problem, the system (e.g. a wall) is modelled as a box with unknown parameters. The system's governing equations are derived and fed by a large-enough set of known outputs and inputs to create a large set of equations. The model may be then identified by finding the parameters which can best satisfy the whole set of equations. As the number of equations are much more than the unknowns, a major challenge in inverse modelling is to research if the thermal system model is identifiable. This can be at risk when the problem does not have a unique solution [8]. Accordingly, the reversibility and the stability of the solution must be checked to identify whether the problem is ill-conditioned. Inverse modelling can be applied to different levels of construction.

1.1. State-of-the-art

1.1.1. Inverse Modelling at Component Level

On the element level (using surface boundary conditions), inverse modelling method with a harmonic approach [9] has been applied to estimate the thermal properties of walls. Specifically, Chaffar et al. [10] used inverse method to characterize homogeneous walls by estimating their thermal conductivity and volumetric heat capacity. Similarly, Rasooli and Itard [11] applied an in-situ method and found the same properties through inverse modelling of a wall's thermal response factors. Šuklje et al. [12] used inverse modelling to characterise green façades and likewise, Deconinck and Roels [13] investigated the ability of stochastic grey-box modelling in characterization of the actual thermal performance of walls suffering from problems such as poor workmanship and consequent phenomena. Their results showed a good agreement between the calculated and the actual R-profiles on frequently-occurring surface temperature differences. Along the same line, Evangelisti et al. [14] used and calibrated a homogeneous wall equivalent to the multi-layered walls using similar techniques.

1.1.2. Inverse Modelling at Building Level

The advantage of using inverse modelling methods on the component level (e.g. walls) is obtaining individual results with high accuracy. However, this requires separate tests and measurements for each parameter in each component of interest. Many of these approaches do not take place due to the hassle and costs associated with their required procedure, calling for automated methods. Following the advancement and growth of sensors and controllers, monitoring of buildings is a new trend [15], leading to the availability of the so called "on-board monitored" data. With regards to this technology, many new buildings and HVAC systems are being equipped with sensors to monitor certain parameters such as air temperature, relative humidity (RH), and CO_2 concentration. Furthermore, with the introduction of smart meters, a huge potential of energy monitoring has been introduced [16,17,18]. With the availability of such large amount of data, using whole building models has become an alternative to component-level measurement methods, especially in cases where more information (e.g. ventilation rate, energy consumption) are simultaneously needed and a very high level of accuracy is not necessarily required. Buildings are accordingly first modelled and analyzed

to predict parameters such as energy consumption, indoor air temperatures, and thermo-physical characteristics.

Inverse modelling has been used in several pieces of research to estimate parameters, leasing to a better prediction of energy behavior. In addition to prediction and characterization of indoor climate [19], numerous studies have been dedicated to estimation of energy demand and energy load calculations through data-driven models. Zhang et al. [20] compared four Inverse Modelling methods for characterization of hot water energy consumption. Similar to these methods, Support Vector Machines [21] and Artificial Neural Networks [22] have been applied to predict energy consumption in commercial buildings. Likewise, An. et al. [23] developed and calibrated an inverse PDE-ODE model and González-Vidal et al. [24] compared a black-box model with a grey-box one for better prediction of the buildings' energy demand. With the same aim, Lam et al. [25] used occupant behaviour data to calibrate an EnergyPlus model for an office building. Braun and Chaturvedi [26] applied a grey-box model and trained it with two weeks of data to accurately predict transient cooling and heating requirements of buildings.

Despite the huge potential and interest in energy load predictions, the application of inverse modelling and machine learning is not limited to this area. Gori and Elell [27] showed the advantage of dynamic grey-box models in reducing the errors when finding the thermal transmittance. Nordström et al. [28] used the energy signature method to estimate the effective U-value of the buildings, showing the possibility of using static energy signature models for sufficiently large indoor and outdoor temperature differences. Most Recently, Senave et al. [29] investigated the level of accuracy in determination of heat loss coefficient through the Average Method [1], Energy Signature Method [30], Linear Regression, and ARX modelling [31]. Along the same line, through sensitivity analysis of the determination of the heat loss coefficient with these methods in another study [32], it was found that the selected input data has a higher impact than the applied data analysis method. Determination of the heat loss coefficient [33–35], also carried out in the current article, is a highlighted issue in the field. During 2017–2021, IEA Annex 71 [36] is dedicated to assess buildings' energy performance by determination of parameters as such. Methods such as QUB [37–39] and ISABELE [40] address the determination of this parameter by conducting in-situ tests. However, these methods require heating pulses to the buildings, implying their feasibility in vacant buildings.

The initial step in inverse modelling is to set-up the most appropriate model that suits the problem. Kramer et al. [41] has compared and categorized building thermal models, suggesting the use of simplified building models with physical meaning. On the one hand, simplified methods benefit from short computation time and lower risk of having multiple solutions. On the other hand, they often fail to present an accurate physical meaning to the identified parameters since they are lumped values of multiple physical parameters. Generally, the models are built and the order can be increased or reduced until a performance criterion is met [42]. Literature shows that the determination of the best model and its solution method is case-specific and depends on the type and operation of the buildings as well as the available input data and the desired outcome. Along the same line, Berthou et al. [43], Hazyuk et al. [44], and Trčka and Hensen [45] showed that the complexity of the model does not necessarily decrease the errors associated with the predictions. Andrade-Cabrera et al. [42] have recently shown a trade-off between the complexity of the lumped parameter models and the energy forecasting accuracy by tracking the annual energy estimation error when reducing a model's complexity. To find the appropriate model, Bacher and Madsen [16] described a hierarchy model selection procedure by likelihood ratio tests and forward selection strategy. The procedure has been applied to a case study to estimate building characteristics such as thermal conductivity and heat capacity. An et al. [46] patented a method consisting of a static model which was achieved by integration of a dynamic model in a long period. By using data regarding temperature, RH and building's information, the thermal properties of the building have been determined. Park et al. [47] used a simple 1R1C (1 resistor-1 capacitor) model to study the internal gains from the appliances in low-energy buildings. A well-insulated room was modelled and measurements were applied to identify the global (lumped) thermal resistance and the global capacitance. The success of the model led to a second study [48] where a 2R2C model was used in combination with an electrical heater to identify the same parameters this time for appliances and for the thermal (building) model. More recently, Zeifman et al. [49] used a second order model rather than a first order one to additionally separate the infiltrative heat loss from the conductive part. More extensively, from 8 different RC models, Ramallo-González et al. [50] found the 2R1C model to work best for their case and was then applied to 6 case studies (houses) to find properties such as the heat loss coefficient. Wang and Xu [51] made an energy model consisting of 3R2C roof, a 2R2C internal mass, and 3R2C external wall to identify the parameters using genetic algorithm (GA) and validated it with an office building. They present the method to simplify energy models using easily available and short-period data. The GA has been often used as a promising optimization technique for the buildings' inverse modelling problems [52]. For instance, Costola et al. [18] used GA to optimize 34 parameters of their model, fed with smart meter energy data, to show the capability of this method in making reliable estimations. However, a trade-off was seen between the variables and the results sets which was said to be solved by using realistic bounds and multiple objective functions. Gupta [53] applied the same method (GA) and fed simulated energy data to a 2R1C, a 3R1C, and a 4R2C model and found the 3R1C to perform better than the other two, in determination of the resistance and capacitance of the buildings.

Over the studied literature, it has been evident that using actual data to estimate building's thermo-physical properties, especially in the occupied residential buildings, has been a well-known significant challenge. Large-scale measurements are always associated with numerous operational and instrumental errors. Accordingly, in comparison with simulated data, using actual data has often led to unsatisfactory results [54]. In the building level, many unidentified random disturbances introduced by occupants influence the energy consumption. Accordingly, many of the studies have dealt with office buildings and commercial buildings where the effects of occupants are limited and therefore easier to model in comparison with residential buildings. In contrast with the majority of the conventional studies which either use synthetic data or study commercial buildings, this research analyses the actual measured data of an occupied residential building.

The advancement and progress of smart meters, sensors and monitoring technologies is leading the building sector to include more and more measurements in their HVAC installations and their control and automation systems. Besides comfort and energy, on-board data from the monitoring of parameters such as temperature, RH, and CO_2 concentrations are of high value in terms of revealing health-related aspects. The aim of this study is accordingly to investigate the possibilities of using such data, in combination with a simple thermal model and inverse modelling, to determine a number of critical global thermo-physical characteristics of an occupied residential building such as the heat loss coefficient, global heat capacity, and global solar effect. It is shown how the different global values of the heat loss coefficient which includes transmission and air exchange (heat transfer by air movement and mixing through ventilation and infiltration) can lead to

better understanding of the buildings' thermal behavior. Furthermore, the importance of using different time periods, period lengths, and granularity levels in the input data are demonstrated showing their effect on the outcomes of the parameter identification. Additionally, it is shown that by using the thermal resistance of buildings' components (either from construction data or from measurements), it is possible to estimate the daily air flow rates of a building in the winter. Finally, the results are evaluated and validated using information available from inspections and construction documents.

Unlike many studies on the same topic, in this research, the procedure regarding preparation, cleaning, filtering, and processing of the data are explained in detail in order to significantly help future similar studies.

1.2. Methodology

The framework of this study begins with measurement of certain parameters in a building. The work continues with construction of a simple 1R1C model representing the building and feeding it with data of different sizes, granularity levels, and time periods, to estimate its global key parameters. An optimization is solved and the parameters are estimated. Thereafter, the building construction information has been applied to find hourly air change rates. The findings are evaluated using the supplementary available information.

To prepare the feed data, first, the indoor air and meteorological measurements were processed and the data has been aggregated in different levels. Then the indoor sensors' data have been calibrated, using the sensors' calibration curves. Thereafter, the energy data were cleaned and filtered using the other sensor's data. The procedure of preparing the data and dealing with missing data points are explained. The required feed data is then prepared: indoor and outdoor average air temperature, total heating consumption, and global solar radiation. Thereafter, the general procedure of making an electrical circuit analogous to the thermal model - according to the available input data and the desired output - is explained briefly for the sake of understanding and examples are shown. With the aim of determination of the building's global thermo-physical characteristics, a 1st order model is built. The model's governing equation (energy conservation) is derived based on the main heat transfer processes. The system's detailed properties are lumped into four equivalent parameters: heat loss coefficient (inverse of global equivalent resistance), global equivalent capacitance, solar gain factor, and a constant parameter (e.g. internal heat generation and other unknown effects). The model is then fed to estimate the four parameters for different periods, durations, and granularity levels (hourly, daily, and weekly values). The parameters are found via inverse modelling of the main equation by defining an optimization problem. The accuracy of the determination of the four parameters cannot be examined as they are lumped parameters and the actual values do not exist. However, using supplementary information such as the construction documents, their range, order of magnitude, and behavior can be evaluated. Finally, the first parameter, the heat loss coefficient, includes a constant part (transmission) and a variable part (ventilation and infiltration). Accordingly, the construction information (based on the building documents or obtained from the measurements) are used to estimate the daily air flow rates in the winter. This is of high importance due to the fact that the ventilation and infiltration in winter times result in considerable values of airborne heat loss in the buildings.

In section 2, the raw data, measuring methods and equipment, and the required processes before feeding the data to the model are explained in detail. In section 3, the chosen model is shown and the inverse modelling of the 1st-order circuit through GA is presented. Thereafter, in section 4, the results are presented and the method is evaluated using the construction documents. Finally, in section 5, conclusions are drawn and recommendations are given.

2. Data: sources, cleaning, and processing

The data used in this study is obtained during a large-scale measurement campaign of 12 months, starting from June 2017. The raw data is obtained in different time intervals. The logging intervals, indoor [55] and outdoor [56] sensor types, instrumentation, and their accuracies are summarized in Table 1.

All logging intervals are synchronized and aggregated to the smallest common available level (hourly data) in the analysis. Since each sensor starts logging at the time it is powered, the logging times are different. Accordingly, the data has been synchronized in such a way that the time shift between the loggings are minimized for all sensors. Indoor measurements have been carried out during a large-scale measurement campaign in the Netherlands [17]. During the campaign, the houses have been inspected and the sensors have been installed in the living room, the kitchen, and the two bedrooms of the houses to measure air temperature, CO_2 concentration, RH, and motion. The sensors used in the houses are shown in Fig. 1.

2.1. Indoor air measurements

The indoor sensors were carefully placed in the most representative locations of the room, avoiding the areas in the vicinity of solar radiation, draught, and moisture. With a logging interval of 5 min, the data were logged for one year. No missing values have been found, thanks to the local memory of the data loggers attached with the sensors. To ensure high accuracy, it is essential to have all sensors recalibrated every 1–2 years. All temperature and RH sensors have been calibrated via a set of pre- calibrated sensors which were individually calibrated in a climate chamber. The calibration has been carried out, having all sensors in a large

Table 1
The description of the sensors by which the data have been measured.

Data	Source	Logging Interval	Sensor Type and Accuracy
Indoor Air Temperature	In-Situ Sensors	5 min	KT Thermistor – 1% per °C (0.15 °C – 0.3 °C)
CO_2 Concentration	In-Situ Sensors	5 min	GE Telaire: 400 – 1250 ppm: 3% of reading
RH	In-Situ Sensors	5 min	Honeywell HiH5031: +/- 3%
Motion	In-Situ Sensors	5 min	Honeywell IR8M: 11 × 12 m (at 2.3 m height)
RH Bathroom	In-Situ Sensors	5 min	Honeywell HiH5031: +/- 3%
Gas Consumption	Smart Meter	1 h	Technolution P1 port reader
Power Consumption	Smart Meter	10 s	Technolution P1 port reader
Outdoor Air Temperature	KNMI	1 h	RTD Pt 500: 0.1 °C
Global Solar Radiation	KNMI	1 h	Pyranometer: 1%
Wind velocity	KNMI	1 h	Cup anemometer: 0.5 ms^{-1}

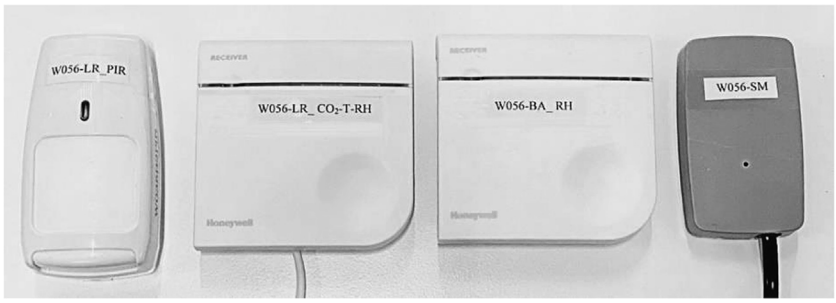

Fig. 1. Sensors used in the measurement campaign, from left to right: motion sensors (4 rooms), CO_2-air temperature-RH sensor (4 rooms), RH sensor (bathroom), and smart meter port reader.

enclosed environment, exposed to two state points, 20 °C – RH 70% and 30 °C – RH 40%. The selected points are chosen based on the operation range of the sensors (indoor environment), assuming a linear correlation between the two points. An example of linear calibration correlations of the sensors are shown in Table 2:

The CO_2 sensors are self-calibrating type and therefore, not manually recalibrated. The instantaneous values of CO_2 concentrations were used only as an indication to the occupants and the evaluation of the findings. In Fig. 2, the results of four parameters measured in the case study (See 3.2) are presented. At the top, left to right, the average room air temperatures and the CO_2 concentration are shown respectively. At the bottom left and the bottom right, average room RH and motion (in binary) are shown for 1 week. The motion measurements help as an indication of presence, showing 0 as no motion and 1 as at least one motion during that hour.

2.2. Meteorological measurements

Meteorological measurements including outdoor air temperature, wind velocity, and solar radiation are provided from the KNMI (Koninklijk Nederlands Meteorologisch Instituut: Royal Netherlands Meteorological Institute) [56]. The local meteorological data is approximated by averaging the measurement values between two nearest stations in province Zuid Holland, both located within 10 km range of the building. These values have shown to be the closest to the actual local values measured via a weather station which has been locally installed after the measurement campaign period. In Fig. 3, local measurements are compared to the assumed (averaged) KNMI values during the same measurement period.

The R^2 values regarding the fit between the KNMI location-based average value, the two locations, and the in-situ measurements for air temperature, solar radiation, and wind velocity are presented in Table 3:

Despite the small difference, the average of the values reported for the two KNMI locations still shows to be the closest to the actual in-situ measurements and therefore has been applied as the input outdoor data.

2.3. Energy consumption recordings and filtering

Energy usage data has been gathered via a Technolution Cloudia smart meter port reader, connected to the P1 port of the smart meter. The logging intervals of the smart meter data from electrical power (kW) and the accumulated gas consumption (m3) are 10 s and 1 h respectively. The hourly rates of heating consumption are found by deducting two consecutive recordings and multiplying by the standard average calorific value of the gas in the Netherlands (35.17 MJ/m^3). The long-time missing values (due to the port reader and communication faults) of the gas and electricity consumption are left blank and not used in the analysis (see Fig. 7). The short period missing values (3–5) hours are filled by the data of the points with similar conditions (e.g. air temperature and time of the day). For shorter periods, the gaps of the missing values have been filled by the average of the values at the beginning and the end of the gaps.

Separation of SH and DHW-related heating from the total heating consumption

The smart meter data shows the hourly total amount of gas consumed for domestic hot water (DHW), space heating (SH), and noise (cooking and boiler set-point heating). Consequently, determination of each category in higher resolution (e.g. per minute) is not possible, unless separate measurements are carried out. Due to the availability of a whole year data in the case study (3.2), rough differentiation between different categories can take place aided by comparing the summer and winter period. During the summer, heating (gas) is not consumed for SH. This knowledge helps in filtering the data in the winter period where both SH and DHW take place. The data due to the DHW can be filtered simply by comparing the magnitude of its peaks in summer. The SH peaks observed in the winter are clearly much larger than the other peaks. The only peaks large enough to be confused with SH values are the shower DHW peaks. Accordingly, the shower times are detected via an RH sensor placed in the bathroom. By observing the data in different period lengths, much information is conveyed. For better observation of the results of filtering and its effect in different scales, Figs. 4–6 are plotted for different durations. In Fig. 4, the bathroom RH (blue) and the total heat consumption (orange) are plotted for 21 days (left), one week (middle), and one day (right) in summer.

To estimate the SH-related heating consumption, the following procedure is carried out:

First, the noise regarding the frequent heating up of the boiler is filtered. This noise is the heat consumed by the boiler to maintain the minimum set point temperature to ensure instantaneous hot

Table 2
Calibration correlations for correction of the measured air temperatures.

Sensor / Readings	Point 1 (°C)	Point 2 (°C)	Calibration Correlation
Pre-Calibrated Sensor	21.2	29.8	–
Temperature Sensor Living Room	22.7	31.9	$T_{correct} = 0.93T_{measured}$
Temperature Sensor Kitchen	22.8	31.0	$T_{correct} = 1.05T_{measured} - 2.7$
Temperature Sensor Bedroom 1	22.7	31.8	$T_{correct} = 0.94T_{measured} - 0.2$
Temperature Sensor Bedroom 2	22.9	31.4	$T_{correct} = T_{measured} - 1.7$

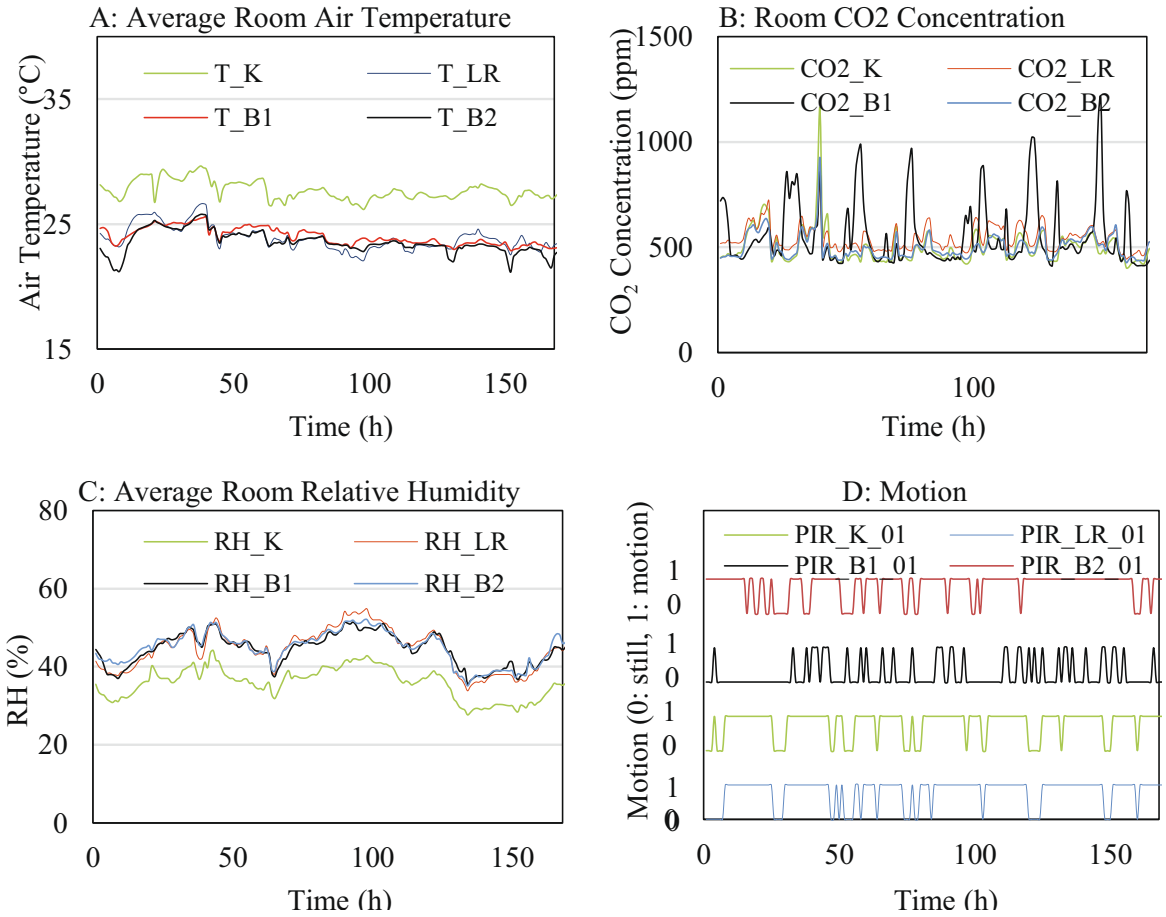

Fig. 2. First week of measurements: room air temperatures (A), room CO_2 concentrations (B), room RH (C) and occupant motion (D) are presented. (LR: Living Room, K: Kitchen, B1: Bedroom 1, B2: Bedroom 2).

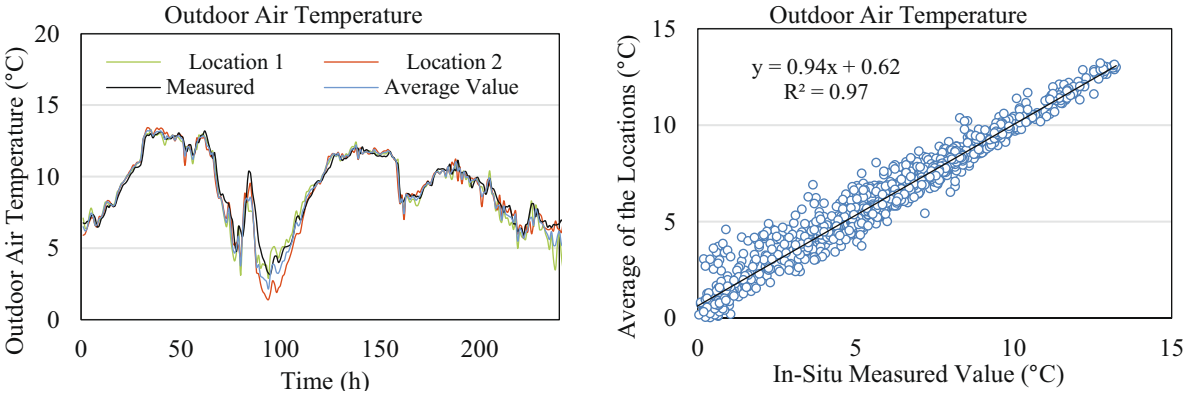

Fig. 3. Comparison between outdoor air temperature data from KNMI in two locations and their average value (the one used in the model) and the in-situ measured values (left – 10 days, December 2018) and the linear regression between the average value and in-situ measurements (right – 56 days).

water supply. Note that the very short periods of using DHW cannot be distinguished from this noise and therefore are eliminated during the noise filtering. Second, all DHW-related heating consumption should be removed from the remaining data to achieve the SH-related heating consumption. Comparing the winter period (frequent SH) with the summer (no SH), the magnitude of the SH and the frequent DHW can be estimated. Ever since the frequent DHW consumption values are much smaller than the SH values and the shower time DHW data points, they can be filtered by omitting the values smaller than a certain level. For this case study, the observed range in summer was 0.9 kW for every hour section. This eliminates the majority of the small DHW-related consump-

Table 3
R2 values in comparison between the parameters in two locations and their average values and the in-situ measured values. December 2018-February 2019.

Location / Parameter	Outdoor Air Temperature	Solar Radiation	Wind Velocity
Location 1	R^2 = 0.96	R^2 = 0.90	R^2 = 0.78
Location 2	R^2 = 0.95	R^2 = 0.90	R^2 = 0.78
Average of the two locations	R^2 = 0.97	R^2 = 0.92	R^2 = 0.81

tions except showering times. Finally, an approximation of the shower DHW consumption can be found following the high peaks of the bathroom RH profile. Accordingly, the heating consumption values taking place during the shower times (when the RH of the bathroom rises above 70%) have been filtered. The same procedure is repeated by filtering based on the RH level at one time step before. This repetition eliminates the consumption from a short period of the hour before. In Fig. 5, the bathroom RH (blue) and heat consumption (orange) raw data (left) and the DHW-filtered one (right) is presented for 21 days of summer.

Similarly, the raw data (left) and the DHW-filtered one (right) is presented in Fig. 6.

Filtering out (the majority of) the DHW-related heating consumption from the total heating consumption (left side in Fig. 6), the SH-related heating consumption is presented (right side in Fig. 6). To validate the filtering methods, the sum of the DHW-related gas consumption (filtered out) is presented as a percentage of the total consumption, in different periods and presented in Table 4. Note that the found values are half of what is assumed in the literature (approximately 20%). However, the difference is explainable due to the low frequency and the short duration of showers (as illustrated from the bathroom RH data and the answers in a separate survey) which are lower than what is assumed in the literature.

The limitation of using hourly data can be mentioned in possible scenarios where the DHW and SH cannot be separated correctly, causing uncertainty:

- The SH starting during a last short period of one hour (e.g. 10:50) and ending at an early period of the logging hour (e.g. 11:10). This results in the peak to break into two smaller peaks which can be confused with DHW use during two hours.
- The case where DHW and SH take place during the same hour.

2.4. Input data for the model

The raw data is processed before being fed to the model of the building (3.2). The average indoor temperature has been obtained from the volume-based average value of the room temperatures. The hourly global solar radiation, initially available in (Jm^{-2}) is converted to (Wm^{-2}) and later to (W) using the transparent surface areas. Finally, the total heating consumption is filtered as explained in Section 2.3 to SH values. The data regarding indoor (top left) and outdoor (top right) air temperatures, total heating consumption (bottom right), and solar radiation (bottom left) are plotted in Fig. 7.

3. Inverse modelling of the building's thermal model

In addition to the statistical methods mentioned in the literature, the choice of model highly depends on the availability of the measured data, the range of parameters, and the desired level

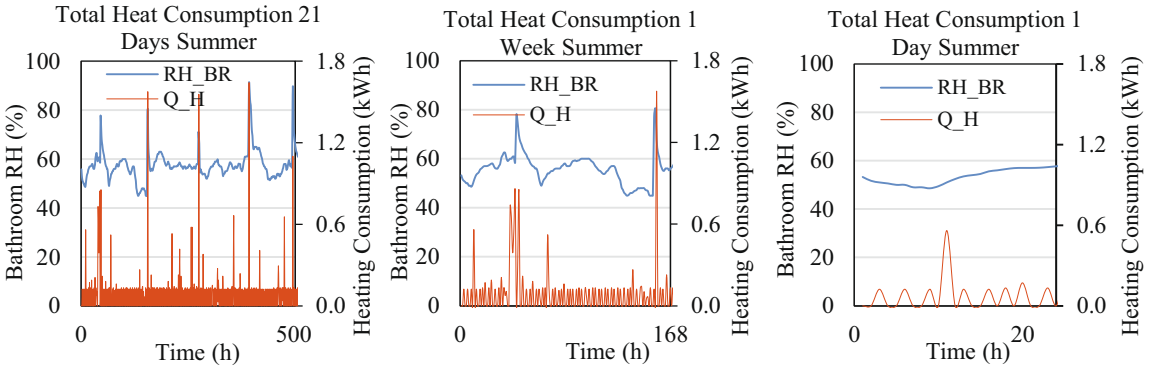

Fig. 4. Total heating consumption, Q_H (in orange) and bathroom RH, RH_BR (in blue) for 21 days of summer. (For interpretation of the references to colour in this figure legend, the reader is referred to the web version of this article.)

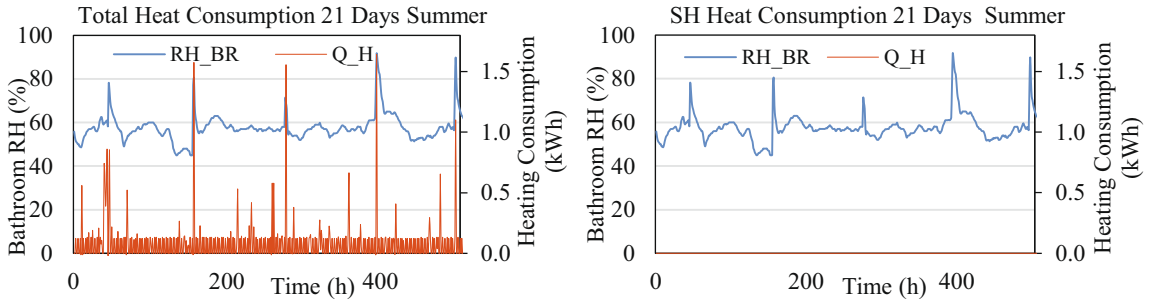

Fig. 5. Bathroom RH (blue) and heat consumption (orange) raw data (left) and the DHW-filtered one (right). (For interpretation of the references to colour in this figure legend, the reader is referred to the web version of this article.)

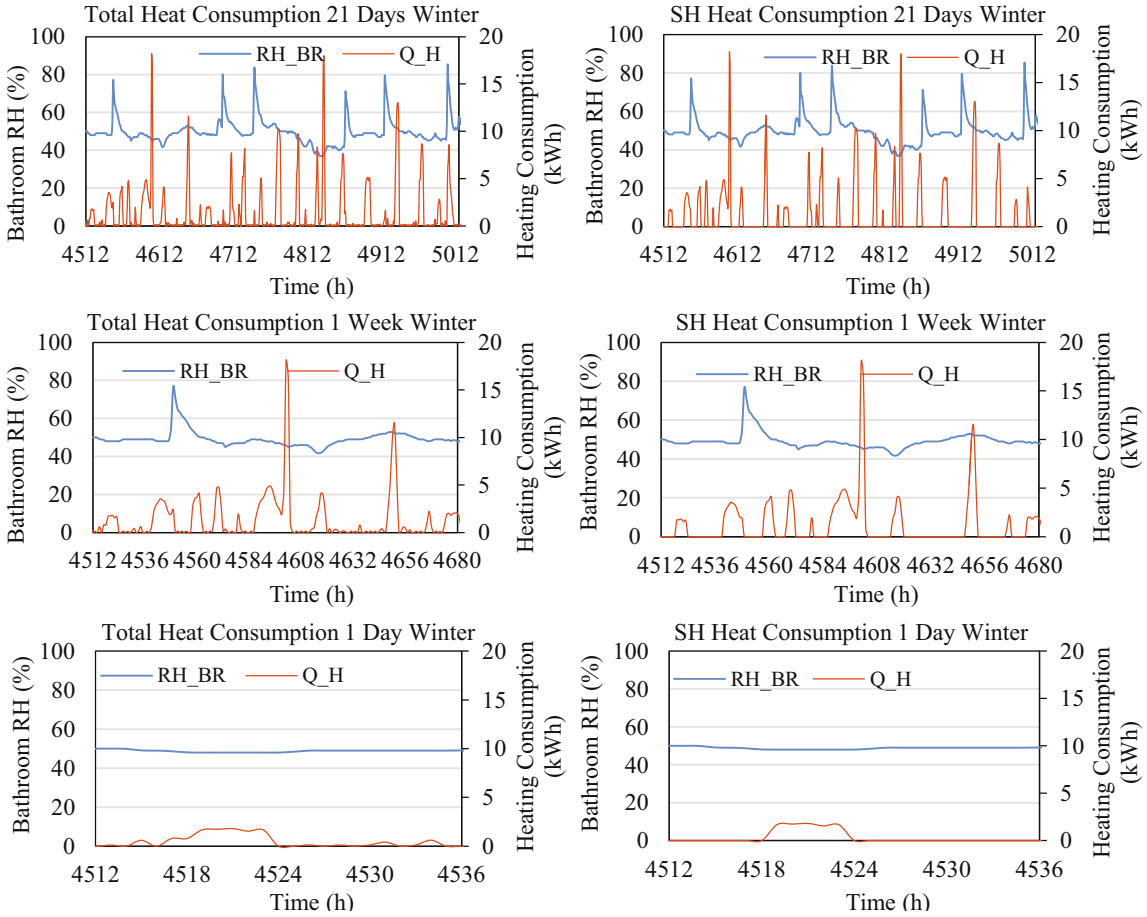

Fig. 6. Bathroom RH (blue) and heat consumption (orange) raw data (left) and the DHW-filtered one (right) for 21 days (top), 1 week (middle), and 1 day (bottom) of winter. (For interpretation of the references to colour in this figure legend, the reader is referred to the web version of this article.)

of outputs (e.g. lumped or local parameters). In Section 3.1 examples of thermal models are shown and in section 3.2 the case study is presented.

3.1. The choice of the model

As already pointed out, there is never a single way of describing the thermal behavior of a building. The use of high-resolution thermal networks requires an abundance of input data and information, which is often not present or cannot be measured. Additionally, with a high-resolution of a model, the chance of finding multiple solutions increases. Accordingly, the accuracy of the estimations does not increase with the increase of the resolution. Therefore, lower resolution models are achieved through model reduction, in which some nodes are neglected or nodes of similar thermal behavior are lumped. A dwelling in a form of detached house for instance, where the sides are in contact with outdoor air, can be modelled in a mid-resolution circuit as shown in Fig. 8 with 11R4C circuit. This model consists of 2 nodes placed on air and 9 on the surfaces of the roof, the floor, the façades (4 orientations). The capacitors (C) are placed on the construction and on the indoor air. Apart from the floor, all components are in contact with outdoor and indoor air. Accordingly, resistances R between the air and the components relate to convective (lumped with IR radiation), and the ones at the boundaries of a circle, relate to conductive heat transfer. Indices *i* and *o* denote indoor and outdoor air and indices H and V indicate horizontal and vertical alignments. When reducing this model, the circles (components) can be taken as single nodes whose conductive resistances are lumped with convective resistance(s). Alternatively, parallel branches can be lumped into a single branch, following the resistance summation rules. Note that the resistance $R_{vent+inf}$ is a variable parameter and therefore has a different value in different periods. Accordingly, when lumping this branch with one with (approximately) constant resistance such as the wall's thermal transmittance, the lumped resistance is also a non-constant.

The same modelling procedure is standard to follow for any type of building. For an apartment, one wall (edge apartment), two walls (middle apartment), or three walls (mid-floor apartment with three neighbors), the floor and the roof (except the highest and lowest floors) are adjacent to the neighbor apartments. Assuming similar indoor temperature in these adjacent media, the heat transfer (air to air) and therefore the thermal resistance R from these components can be neglected in the calculations. In an apartment in the middle floors, two main nodes can be considered: the interior air and the exterior air. The nodes are connected via resistors and internal nodes, the surface temperatures. The thermal mass capacitors are the same as the house. In Fig. 9, an example electrical circuit analogous example to the case study apartment is shown.

According to Kirchhoff's current law, the sum of the currents towards a node (e.g. air) are equal to zero:

$$\sum I = \frac{1}{R}\,\Delta V_0 + \mathrm{C}\,\frac{\partial V_0}{\partial t} + I_{source} = 0 \qquad (1)$$

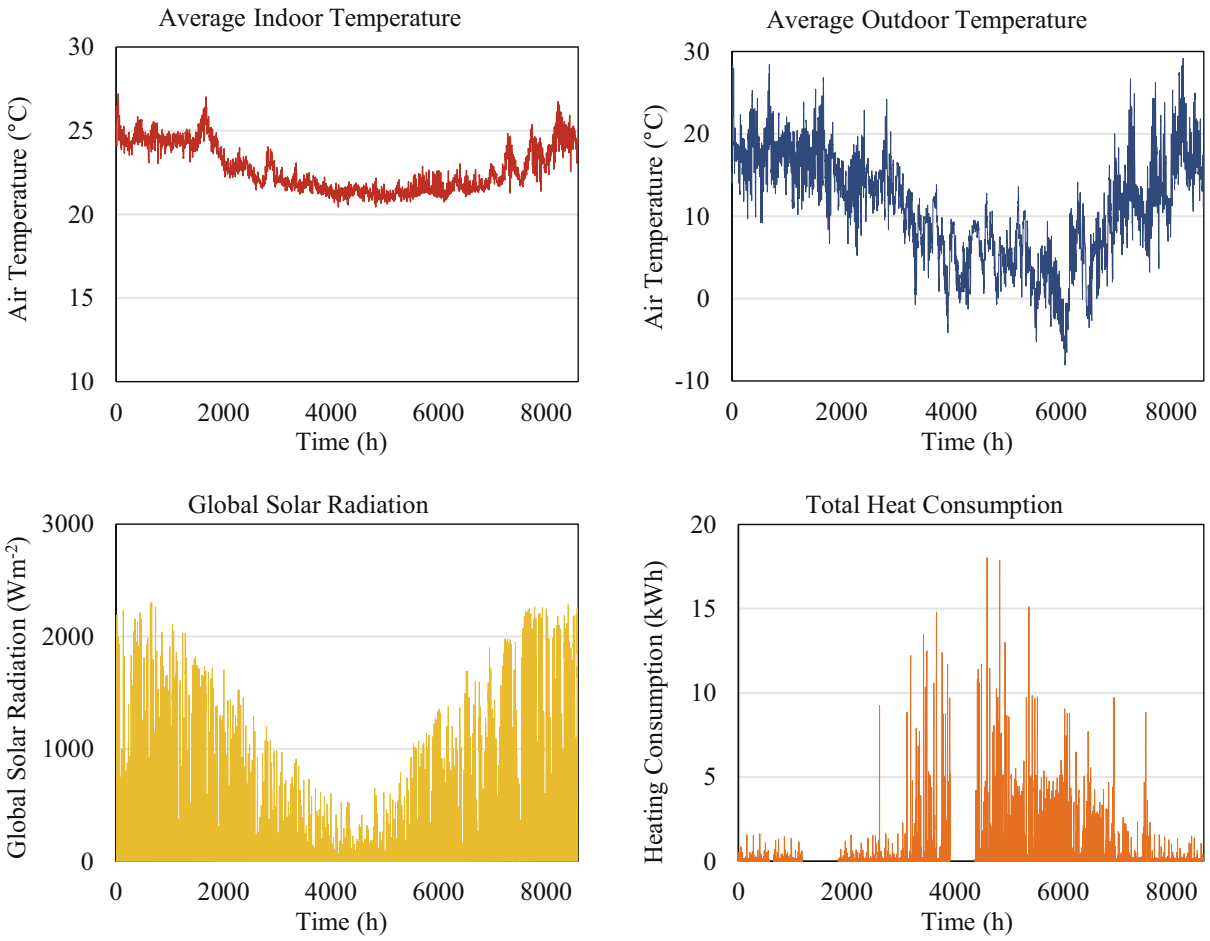

Fig. 7. Indoor (left top), outdoor (right top) air temperatures, Solar radiation (bottom left), and the total heating consumption (bottom right) for one year in the case study.

Table 4
Total, SH-related and DHW-related gas consumption in different periods.

Duration	Total heating consumption (kWh)	SH- heating consumption (kWh)	DHW to total gas consumption (%)
7 Days	230.21	211.62	8.07
21 Days	716.07	636.86	11.06
2 Months	1925.77	1747.20	9.27
3 Months	2849.30	2591.38	9.05

where ΔV_0 is voltage drop, R is resistance, C is capacitance, and I is the electrical current. Following the analogy between the circuit and the thermal system (the building), the currents (heat flow) can be computed from the voltages (temperatures), resistances (thermal resistances), and capacitances (thermal masses). This is in fact a visualization of what was always done in building simulation.

Of the most important parameters defining the resolution of the model, is the feed data, which should match not only the physics involved, but also, the available level of detail in the input and output data. Finding a balance between the desired accuracy and level of outputs, the available data, and the potential of the model to be identifiable, one can make an appropriate choice of the model's resolution. Note that in high resolution models, the risk of finding multiple sets of answers increases and therefore these models are not always suitable for inverse modeling [41].

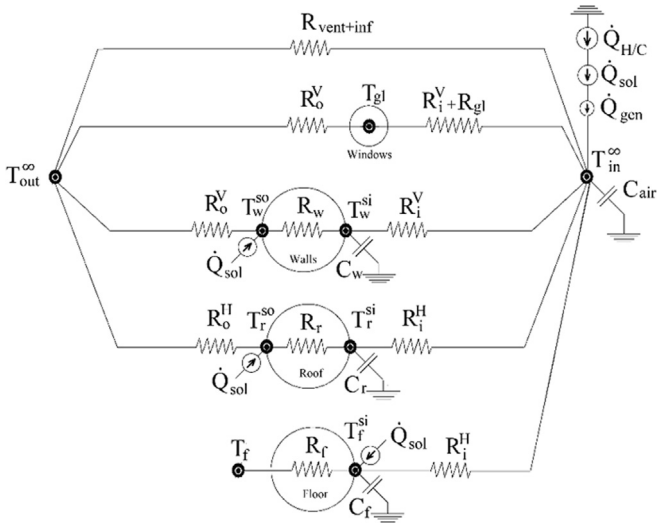

Fig. 8. The 11R4C model for a detached house: Thermal resistances and capacitances are modeled as resistors and capacitors.

3.2. The case study

The case study building is one-floor, four-room apartment of 72 m^2, located in the West of the Netherlands. The building construction year is 2014 and certain standards regarding the energy

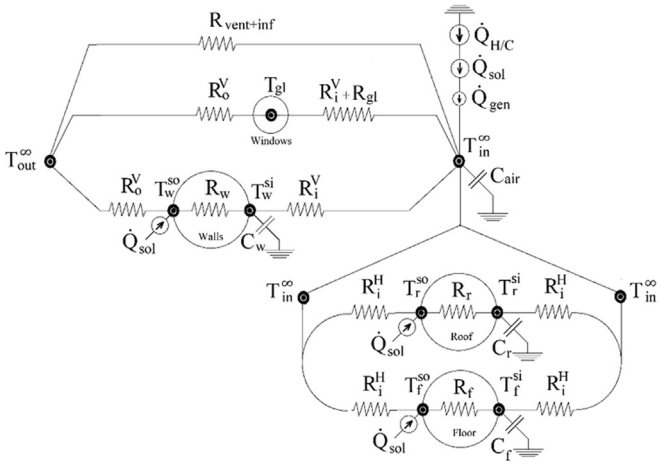

Fig. 9. The 12R4C model for a mid-floor apartment.

efficiency have been carefully followed (Energy label A: windows HR++, the façade walls' and the roof's thermal resistances 4 $m^2K^{-1}W^{-1}$ and 5 $m^2K^{-1}W^{-1}$ respectively). The apartment unit is adjacent to two neighbors on west and east sides and has a south façade and a north façade which faces the patio. The heating system is a combination condensing boiler which heats all 4 rooms. The thermostat is set at 21 °C at all times. For the input data, the air temperature is taken from the measurements and not the thermostat settings. The house is occupied all day, by a single middle-aged occupant, and is ventilated via a mechanical ventilation system at medium stand. The indoor air temperature of four rooms are available whereas no surface temperature has been measured. Accordingly, a zonal model with four indoor air nodes as shown in Fig. 10 is a better choice than the one previously shown in Fig. 9.

As seen in Fig. 10, due to the lack of data of the surface temperatures, the corresponding nodes are omitted. Therefore, the capacitors and resistors are lumped parameters of more detailed actual ones.

3.3. Building the 1st – order circuit

The aim here is to apply the simplest model that can work with minimum measurements (e.g. no surface temperature data) to estimate parameters such as the heat loss coefficient. Reducing the circuit to the simplest possible dynamic model, a 1R1C model

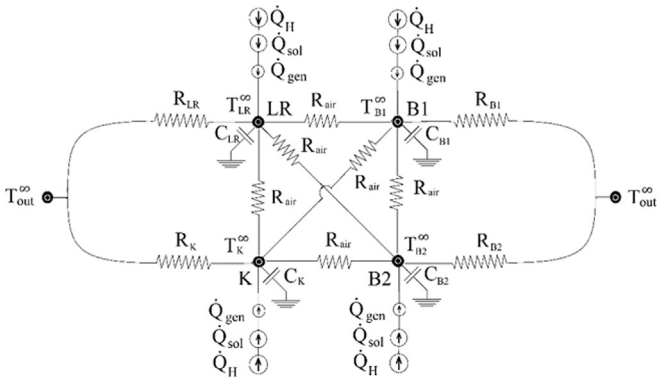

Fig. 10. The high-resolution electrical circuit model analogous to the case study, according to the available measured data.

is built, shown in Fig. 11. This model is used in the inverse modelling of its four global parameters, using the available input and output data. Analogous to the thermal system (the building), the building's resistance against transmission and advection heat loss/gains translated into an equivalent global thermal resistance R_{eq} , including the resistance of all exterior walls, roof and floor, ventilation and infiltration. Similarly, equivalent thermal capacitance C_{eq}, represents the buildings total equivalent thermal mass, showing the dynamic ability of the system to accumulate/release heat. Note that this capacitance is not the air capacitance but reflect the behaviour of the building (air + construction). Other heat sources such as internal gains are taken as a separate flow source $\dot{Q}_{gen}$ in the circuit. S_0 indicates the portion of solar heat that enters the system.

The state equation of this system, based on energy conservation is as follows:

$$\left(\dot{Q}_{advection} + \dot{Q}_{transmission}\right) + \dot{Q}_H + \dot{Q}_{sol} + \dot{Q}_{gen} = \dot{Q}_{storage} \tag{2}$$

where the sum of the heat flows is stored in the system. It is of high importance to state the model equation in such a way that in the governing equations, parameters would not have the possibility to compensate for each other during the inverse modelling. Deriving the energy conservation equation for indoor air, the following equation is obtained:

$$\left[\left(\rho c_p \dot{\forall}\right)_{air} + \sum_{i=1}^{4} U_i A_i\right]\left[T^{\infty}_{out} - T^{\infty}_{in}\right] - \sum_i \frac{\partial T}{\partial t}(\rho c \forall)_i + \eta.\left[\dot{Q}_H\right] + \left[\dot{Q}_{sol}\right] + \left[\dot{Q}_{gen}\right] = 0 \tag{3}$$

where U is the thermal transmittance (air to air) of each building envelope component, T is the air temperature, ρ is the density, c_p is the specific heat capacity, $\forall$ is the volume, $\dot{Q}_H$ is the heating consumption recorded by the smart meter, η is the nominal efficiency of the boiler which according to the manual of the boiler is taken as 0.9, $\dot{Q}_{sol}$ is the global solar radiation, A is the surface area, t is time, and i is the index for different components which accumulate heat (walls, celling, floor, and air). Note that here it is not possible to separate air advection heat transfer from transmission losses as the driving forces are the same. Taking a global equivalent resistance between indoor and outdoor air, R_{eq}, and a global capacitance C_{eq} which stores and releases the heat from/to the air and the construction, (6.3) can be translated to the following:

$$R^{-1}_{eq}\left[T^{\infty}_{out} - T^{\infty}_{in}\right] - C_{eq}\left[\frac{\partial T^{\infty}_{in}}{\partial t}\right] + \eta.\left[\dot{Q}_H\right] + S_0.\left[P_{sol}\right] + S_1 = 0 \tag{4}$$

In which R^{-1}_{eq} is the heat loss coefficient, S_0 is the average fraction of the solar irradiance that enters the system and influences the indoor air, and S_1 is a constant for all the other effects including the internal heat gains. The global heat loss coefficient R^{-1}_{eq} is the equivalent summation of all transmission resistances and ventilation advection resistances:

$$R^{-1}_{eq} = \frac{1}{R_{vent}} + \sum \kappa_{f,\ r,\ w,\ g} = \left(\rho c_p \dot{\forall}\right)_{air} + (UA)_w + (UA)_r + (UA)_{gl} \tag{5}$$

where floor is neglected due to the existence of adjacent unit with similar indoor temperature. The storage parameter C_{eq} is an indirect equivalent thermal mass of the system, roughly approximated by:

$$C_{eq} \equiv \left(\rho c_p \forall\right)_{construction} + \left(\rho c_p \forall\right)_{air} \tag{6}$$

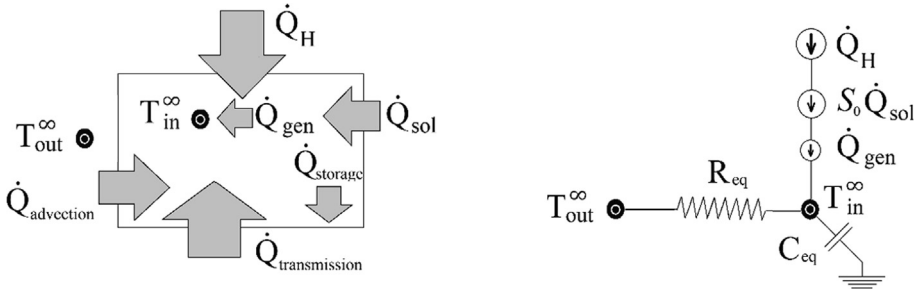

Fig. 11. The first order model: 1R1C analogized electrical circuit with two nodes of air temperatures (indoor and outdoor) heat transfer phenomena are the electrical currents towards the indoor air node.

where $\rho c_p \forall$ is the thermal mass of the construction (floor, roof, walls, and internal walls) and of the air. Where $\rho c_p \forall$ is the thermal mass of the construction (floor, roof, walls, and internal walls) and the air.

The parameter S_0 is taken as a fraction of the global solar radiation transmitted through the windows. Accordingly, the heat penetration to the system via solar radiation can be computed as following:

$$\dot{Q}_{sol} = S_o.A_{gl}.P_{sol} \tag{7}$$

where A_{gl} is the total glass surface and P_{sol} is the global solar irradiance. Note that S_0 should not be confused with the g-value of the glass, in this building equal to 0.58 (HR++ type). The first, shows the seasonal/daily fraction of solar radiation, entering the house and affecting the heating consumption and indoor temperature, whereas the latter is a constant window property. The advantage of using S_0 rather than the g-value is that the S_0 is based on the specific building and not solely on the window.

3.3.1. Objective function and inverse modelling

The generic definition used for inverse modelling can be stated as following:

A recording the actual inputs $u(t)$ and outputs $\mu(t)$ is available. A prediction $\mu^{th}(t,\ \theta)$ is then generated by feeding $u(t)$ to a model consisting of parameters θ. Inverse modelling takes place by determining the parameter vector θ_{eq} that minimizes a (usually quadratic) norm (σ) of the predicted error [57]:

$$\theta_{eq} = \underset{\theta}{\operatorname{argmin}} \sum_{t} \sigma(\mu^{th}(t,\ \theta) - \mu(t)) \tag{8}$$

To incorporate the long-time dynamic effect of the thermal mass, the state equation targets indoor air temperature. Accordingly, for the current problem, θ_{eq} is the vector $[R_{eq}^{-1}\ \ C_{eq}\ \ S_0\ \ S_1]$ which is estimated from the input $u(t)$ being the heating consumption, outdoor temperature, and solar irradiance, and the output $\mu(t)$ the indoor air temperature. The prediction function is then as following:

$$T^{\infty}_{in}\big|^{th}_{t} = \left(\eta\dot{Q}_H + \frac{1}{R_{eq}}\left[T^{\infty}_{out}\right] + S_0\dot{Q}_{sol} + S_1\right) + C_{eq}\left[T^{\infty}_{in}\big|^{th}_{t-1}\right]\Bigg) \Big/ \left(\frac{1}{R_{eq}} + C_{eq}\right) \tag{9}$$

The objective is to minimize the norm (σ), taken as the RMSE (Root Mean Square Error) between actual and theoretical indoor air temperature. The objective function of the optimization problem is accordingly stated as follows:

$$\min_{\frac{1}{R_{eq}},\ C,\ S_0,\ S_1} \sqrt{\frac{1}{n}\sum_{i=1}^{n}\left(\left(\eta\dot{Q}_H + S_0\dot{Q}_{sol} + S_1 + \frac{1}{R_{eq}}\left[T^{\infty}_{out}\right]_i + C_{eq}\left[T^{\infty}_{in}\big|^{th}_{t-1}\right]_i\right)\left(\frac{1}{R_{eq}} + C_{eq}\right)^{-1} - T_i^{ac}\right)^2} \quad \text{s.t. } R_{eq}^{-1} \in [10,\ 180];\ C_{eq} \in [1\text{E}5,\ 1\text{E}9];\ S_0 \in [0,\ 1];\ S_1 \in [0,\ 2000] \tag{10}$$

Table 5
Upper and lower bounds of the parameters defined in the optimization problem.

Parameter	Lower Bound	Upper Bound
R_w	0.2(m^2KW^{-1})	8 (m^2KW^{-1})
R_r	0.2(m^2KW^{-1})	8 (m^2KW^{-1})
R_{gl}	0.1 (m^2KW^{-1})	0.7 (m^2KW^{-1})
ACH	0.1 (h^{-1})	2 (h^{-1})
$\left(\rho c_p \dot{\forall}\right)_{air}$	6.8 (WK^{-1})	145 (WK^{-1})
$1/R_{eq}$	10 (WK^{-1})	180 (WK^{-1})
$(\rho c \forall)_{construction}$	8 E6 (JK^{-1})	4 E7 (JK^{-1})
S_0	0	1
S_1	0	2000

Ranges of the global parameters presented in the constrains are estimated based on the possible ranges of the physical properties they are computed from. The possible ranges of the properties in building industry are presented in Table 5. Note that the global R and C are found case-specific since the surface areas are included in the calculation. The surface areas used in the calculations are presented later in Table 8.

The optimization problem presented is solved using GA through MATLAB. Using other methods including Quasi-Newton and interior-point have resulted in nearly the same values and therefore are not presented here. Customized settings used for the GA are population size of 20000, generations of 4000. The mutation and crossover values are the default ones in MATLAB. The results of the optimization in this problem have shown to be insensitive to the changes of these values. As the GA, due to its stochastic nature, does not lead to a unique solution, the optimization is run multiple times and the solution with the lowest objective function value (RMSE) is reported. The variation in the results has not been significant.

3.3.2. Granularity level, time period, and the size of the input data

The model has been fed with the data from different periods and granularity levels. First, the data from the whole year and then the data from the available two months of winter period (January-February) are fed to the model. Then, the data is reduced from one month (February) to the data from two weeks, one week, and finally one day in February 2018. February is chosen here because it is statistically known to be the coldest month of the year in the Netherlands. Separately, data from November and January are used to examine the method's performance. The meteorological winter is defined as December- January- February. However, due to the large energy data gaps in December 2018, this month unfortunately could not be used. For each period, hourly, daily, and weekly data has been fed to the model. Using different periods and granularity levels, the method can be validated in terms of precision and the performance of the method as a function of input data can be expressed.

4. Results and discussion

The outcomes and the results of the inverse modelling are presented here. The findings and outcomes are later evaluated using the construction data taken from the energy and construction detailed reports and the floor plans available from the municipality. For this case, due to the construction year and the quality of the reports and the corresponding organizations, this data has appeared to be reliable.

4.1. Outcomes of the inverse modelling

For each of the mentioned periods, the problem has been solved using different granularity levels of hourly, daily and weekly (when applicable). The results of the optimization are presented in Table 6.

To test the reliability of the method further, data sets from two other periods have been tested. In Table 7, the outcomes of the optimization for November 2017 and January 2018 are presented.

As seen in Tables 6 and 7, the first parameter R_{eq}^{-1} takes different values when different periods are used. These differences are attributed to the different infiltration and ventilation rates in different periods. The average values of hourly, daily, and weekly heat loss coefficient are in a close range. Opposite to this, the values of C_{eq} become smaller in lower granularities (e.g. weekly), showing the weakening of the dynamic effect when analyzing longer time periods. From building physics point of view, it is known that the response time of the buildings is in the order of days. Accordingly, using low granularity levels (daily/weekly), the dynamics cannot be captured. Consequently, in terms of granularity level, the use of hourly data is expected to result in the best estimation of C_{eq} in this problem. Note that the determination of the second parameter, $C_{eq}$is not always reliable, due to its high magnitude in the equation: a small temperature measurement error (inevitable in measurement equipment) multiplied by the large C_{eq} results in a large difference in its term in the equation. Generally, when building a model with one capacitance, the C_{eq} will have a large quantity and therefore less accurate, whereas in a higher resolution of model, the capacitance breaks down into smaller ones in each component, leading to higher accuracy. This is in agreement with the findings of Bacher and Madsen [16]. The solar factor S_0 remains below 1 and varies in different values and when analyzing hourly, daily, and weekly data due to the difference in averaged and detailed data points and the difference in gain in different periods of the year. Similarly, the last parameter, S_1 varies in different granularity levels and periods, giving an indication of the heat generation and other changes in the system (e.g. occupant behavior) which have no correlation with the air temperature, temperature change, and solar radiation. The obvious sources of uncertainty for this method include:

- The choice of model in terms of resolution and lumped parameter modelling
- Limitation in addressing any level of the stochastic user behavior in the model
- Assumption of constant parameters such as heat transfer coefficients and air exchange rates
- The uncertainty of the measured data and the choice of processing (e.g. using average indoor temperature)
- The uncertainty of the SH filtering of the heating consumption data.
- Averaging variable parameters including S_0, S_1, and R_{eq}^{-1}.

The method in general works best for the coldest months of the year (winter) attributable to the large sizes of peaks in energy data. Such data helps in better training of the model. Additionally, for the same reason, the filtering of the DHW is also more accurate during the winter period. Using warmer periods, the heating values are in a smaller range and steadier, which results in inaccurate DHW data filtering and a poorer training of the model. This issue amplifies especially in a well- insulated house, such as the case study, where the indoor air temperature is stable. The summer period is not discussed due to the lack of heating consumption data. In the summer period, the heating is off, no cooling takes place (in the Netherlands), and manual ventilation generally occurs more often through the windows and doors. Using the results of the optimization, a predicted temperature function is fitted to the actual one. The results of the comparisons are presented in Fig. 12. The hourly (on top) and daily (bottom) data have been fed to the model. The estimated

Table 6
Results of the optimization for different period lengths using different granularity levels.

Duration	Granularity Level	R_{eq}^{-1} [WK^{-1}]	C_{eq} [JK^{-1}]	S_0 [–]	S_1 [W]	RMSE [K]
Complete year June 2017-June 2018	Hourly	81	3.4E 8	0.10	98	0.95
	Daily	82	1.5E 7	0.10	114	0.89
	Weekly	81	1.6E 6	0.10	88	0.78
2 months winter: January-February 2018	Hourly	148	1.7E 8	0.30	994	0.21
	Daily	148	7.2E 7	0.55	676	0.18
	Weekly	149	1.0E 7	0.20	1399	0.05
1 month: February	Hourly	138	1.4E 8	0.25	914	0.26
	Daily	138	1.6E 7	0.20	1222	0.10
2 Weeks: February 1–14	Hourly	115	2.1E 8	0.48	60	0.19
	Daily	110	1.2E 7	0.31	310	0.02
1 Week: Feb 1–7	Hourly	157	2.0E 8	0.66	486	0.13
	Daily	148	1.1E 7	0.55	697	0.03
Day 1 Feb	Hourly	100	1.0E 8	0.34	72	0.10

Table 7
Results of the optimization for November 2017 and January 2018 using different granularity levels.

Duration	Granularity Level	R_{eq}^{-1} [WK^{-1}]	C_{eq}[JK^{-1}]	S_0 [–]	S_1 [W]	RMSE [K]
November 2017	Hourly Daily	101	2.0E 8	0.25	169	0.18
		108	2.9E 7	0.42	56	0.09
January 2018	Hourly Daily	128	2.3E 8	0.80	125	0.21
		130	3.1E 7	0.90	44	0.13

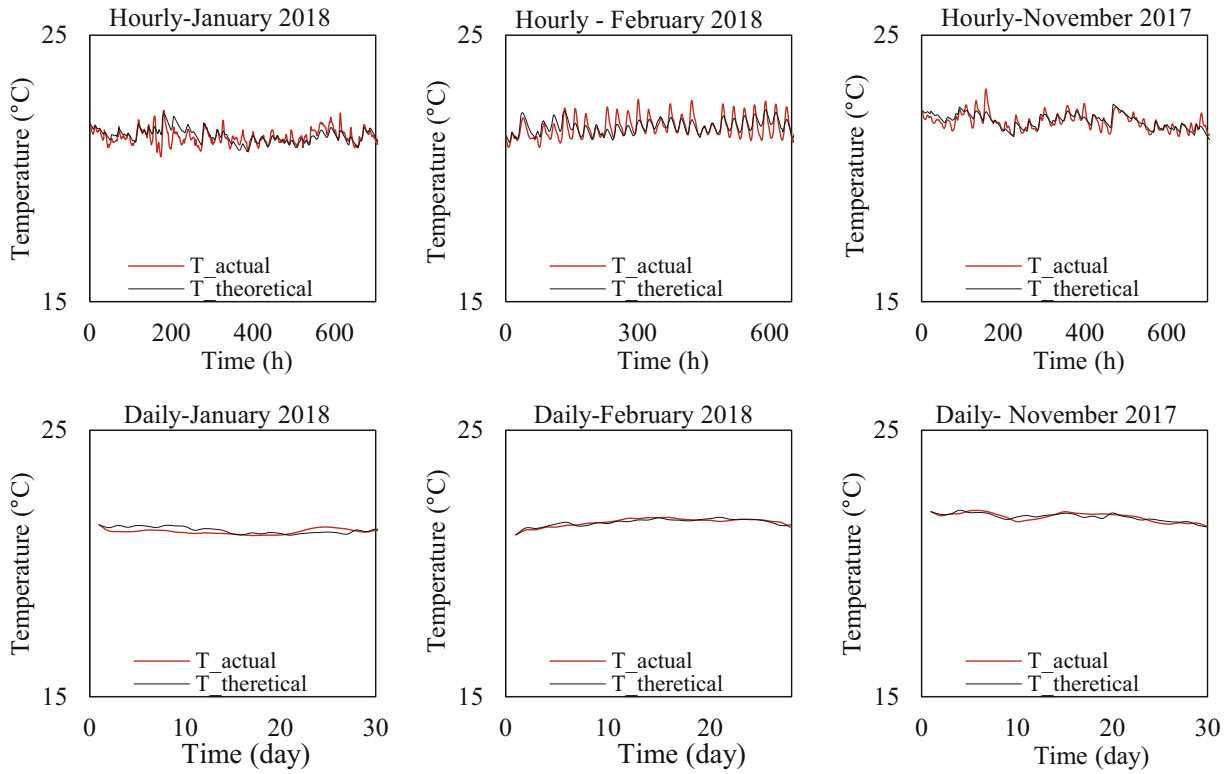

Fig. 12. Actual and computed hourly (top) and daily (bottom) estimated (in black) and actual (in red) temperatures for January 2018 (left), February 2018 (middle), and November 2017 (right). (For interpretation of the references to colour in this figure legend, the reader is referred to the web version of this article.)

temperatures (in black) and the actual temperatures (in red) are shown for January 2018 (left), February 2018 (middle) and November 2017 (right). As seen in Fig. 12, for the hourly data, opposite to the trend which is well captured, the peaks are not always well predicted. Using daily data, a good agreement is seen between the actual and theoretical (computed) values of temperature.

The same procedure is repeated and shown in Fig. 13, by using hourly (left), daily (middle), and weekly (right) data for two months of January 2018 and February 2018:

4.2. Evaluation based on the construction data

The outcomes of the optimization are only average values of variable parameters. To evaluate the findings of the models and analyses, the results are compared to the actual approximation of the parameters based on construction data. The properties of the components and parameters needed in the evaluation are obtained from the inspections and the official construction report documents (energy report) and are tabulated in Table 8. Note that the thermal capacitance values (right column) are roughly approximated from the construction materials and have not been mentioned in the reports. The missing values (e.g. floor's R_c-value) are the ones that have not been relevant for this case study.

As for the first parameter, the inverse equivalent resistance (heat loss coefficient) R_{eq}^{-1} should be equal to the inverse summation of the parallel resistances:

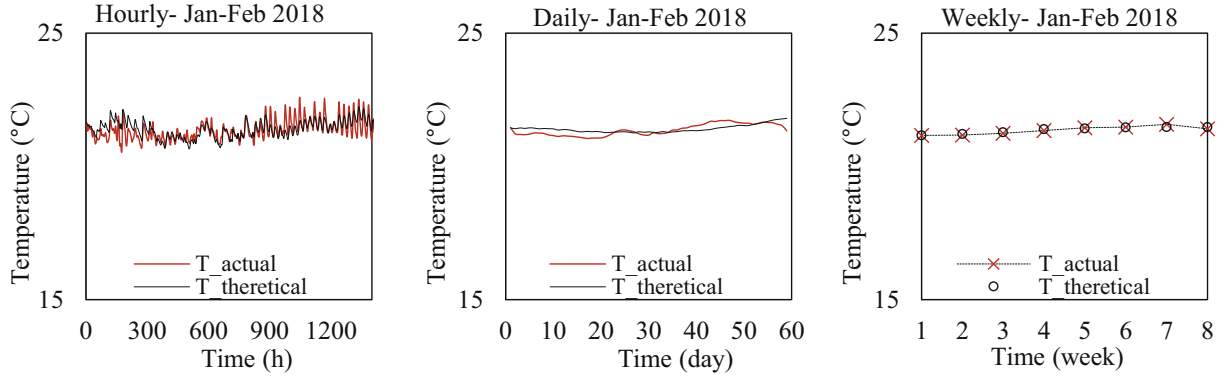

Fig. 13. Actual and computed hourly (left), daily (middle), and weekly (right) temperatures for two months of January 2018 and February 2018.

Table 8
The building's components and their properties.

Component	Area (m^2) – Volume (m^3)	Type-Configuration	R_c (m^2KW^{-1})	$\rho c_p \forall$(WK^{-1})
North window	8 (m^2)	HR ++ (4–15-4)	0.55	–
South window	5 (m^2)	HR ++ (4–15-4)	0.55	–
Side walls	52.4 (m^2)	Reinforced Concrete	–	3.3E7
Opaque façade	26.2 (m^2)	Insulated Brick and Gypsum	4	1.3 E7
Roof	72 (m^2) – 21.6 (m^3)		5	4.5 E7
Floor	72 (m^2) – 21.6 (m^3)	Insulated Concrete	–	4.5 E7
Internal Walls	133.4 (m^2) – 14 (m^3)	Insulated Concrete	–	1.1 E7
Indoor Air	195 (m^3)	Gypsum Properties at 21° C	–	2.4 E5

$$R_{eq}^{-1} = \rho c_p \dot{\forall}_{air} + \frac{A_r}{(\alpha^H_i)^{-1} + L_r k_r^{-1} + (\alpha^H_o)^{-1}} + \frac{A_w}{(\alpha^V_i)^{-1} + L_w k_w^{-1} + (\alpha^V_o)^{-1}} + \frac{A_{gl}}{(\alpha^V_i)^{-1} + L_{gl} k_{gl}^{-1} + (\alpha^V_o)^{-1}} \quad (11)$$

where the α is the convective (lumped with IR radiation) heat transfer coefficient with superscripts V as vertical and H as the horizontal orientations. Due to the small influence of this parameter in the R_{eq}^{-1} and its limited range, here it has been taken as a constant with the average values (common values often used in the literature and building simulation) shown in Table 9:

According to the values of Table 8 and Table 9 in equation (11), the actual range of the heat loss coefficient R_{eq}^{-1} for the specific building can be estimated.

In this case study, the transmission part of the heat loss coefficient is relevant only for the North and South opaque facades, the roof, and the windows with a total value of 37 WK^{-1}. The expected range is therefore as follows:

$$\begin{cases} \frac{1}{R_{eq}} \approx 65 + 5.25 + 13.68 + 18 = 102 \ \ WK^{-1} & at\ 1\ ACH \\ \frac{1}{R_{eq}} \approx 97.5 + 5.25 + 13.68 + 18 = 134.5 \ \ WK^{-1} & at\ 1.5\ ACH \\ \frac{1}{R_{eq}} \approx 130 + 5.25 + 13.68 + 18 = 167 \ \ WK^{-1} & at\ 2\ ACH \end{cases} \quad (12)$$

According to the building's air tightness report, the air rate is is approximately 95 WK^{-1}. Summing up this value with the transmission resistance, an average heat loss coefficient of 132 WK^{-1} is expected. Values obtained from the model show a maximum of 23% deviation with this value. Note that the heat loss coefficient is not a constant due to the variable ventilation and infiltration rates in addition to the occupant-related air exchange rates. Accordingly, the assumed value is just an indication of the possible range of this parameter. Similarly, the global capacitance C_{eq} is roughly approximated from the summation of all heat storing components, assuming the indoor air and the construction as a single node and therefore the same behavior:

$$C_{eq} \equiv (\rho c \forall)_f + (\rho c \forall)_w + (\rho c \forall)_{gl} + (\rho c \forall)_r + (\rho c \forall)_{internal\ \ walls} + (\rho C_p \forall)_{air} \quad (13)$$

In which the air has the smallest thermal mass. According to the values in Table 8, the global capacitance takes a minimum value of 1.5 E8 JK^{-1}. This value is expected to be higher due to the solids other than the construction (e.g. furniture). The values obtained from the model show to be in the expected range. However, the exact value of the capacitance cannot be discussed here as a consequence of the assumptions made and the simplicity of the model. The third parameter, the solar gain fraction S_0 requires in-situ measurements. However, the obtained range of [0 1] as expected from the physics point of view (only a fraction of solar radiation heats the building) confirms the relative validity of the findings. The last parameter S_1 is not evaluated due to the limited knowledge regarding the actual internal gains and unknown effects in the case study. In all cases, this value has taken a positive number, showing the positive rate of heat generation in the system.

Table 9
Indoor and outdoor assumed average convective heat transfer coefficients.

Property	Vertical α^V ($Wm^{-2}K$)	Horizontal α^H ($Wm^{-2}K$)
Indoor convective HTC	7.5	7.5
Outdoor convective HTC	25	18.5

4.3. Determination of air flow rates

In the previous section, an average global heat loss coefficient was sought. This parameter includes a fixed part (relating to transmission losses assuming constant convection heat transfer coefficients) and variable parts relating to air exchange and movement (ventilation and infiltration). In the current case study, according to the survey, occupancy and the user behavior during the weekdays is the same as in the weekends. Accordingly, here, it is assumed that the major part of the changes in the daily change of energy use are associated with variations in air change rates. Obtaining the global capacitance, solar fraction, and the internal gain from the optimization, the ventilation and infiltration rates can be estimated by recalculating the heat loss coefficient by the following equation:

$$\left[\frac{1}{R_{eq}}\right]_i = \frac{C_{eq}\left(\frac{\partial T^{\infty}_{in}}{\partial t}\right)_i - \eta . \left[\dot{Q}_H\right]_i - S_0 . \left[\dot{Q}_{sol}\right]_i - S_1}{\left[T^{\infty}_{out}\right]_i - T^{\infty}_{in}\big|^{th}_i} \quad (14)$$

In which, the differentiation has been approximated, using high-order approximation central difference, using 5 points (two before and two after):

$$\left(\frac{\partial T^{\infty}_{in}}{\partial t}\right)_i = \left(-T^{\infty}_{in}\big|_{t+2} + 8\ T^{\infty}_{in}\big|_{t+1} - 8\ T^{\infty}_{in}\big|_{t-1} + T^{\infty}_{in}\big|_{t-2}\right)/12\ \Delta t + \mathcal{O}(\Delta t)^4; \quad \Delta t = 1\ (h) \quad (15)$$

Computation of the daily heat loss coefficient rates, term R_{eq}^{-1} can be found. Here, the daily rates are used rather than hourly rate due to the better fit shown in Fig. 12 and the absence of undesired meaningless noise. The outcomes of (14) are presented in Fig. 14. Note that the first and last two days are not presented here due to the discretization method used in (15) which uses 2 days before and after the current time. In case of using another discretization method (e.g. forward with one point), these days can also be added to the estimations. For lower granularity levels (e.g. week), the capacitance term can be neglected.

Using (11), and the resistance properties of the construction (the transmission part of 37 WK^{-1}), the air change rate fraction can be separated. Using (12), these values are converted to air flow rates (ACH) and plotted in Fig. 15. Note that for an old

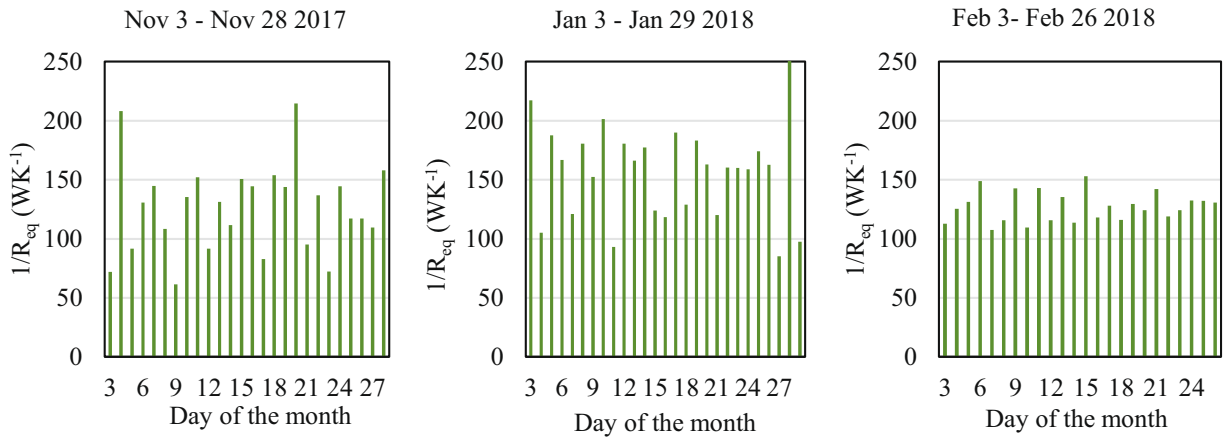

Fig. 14. The computation results of the heat loss coefficient for November 2017, January 2018, and February 2018.

building where the construction is unknown, the thermal resistances or the thermal transmittances of the façades can be measured following a measurement method (e.g. ISO 9869 [1]). This needs the same time as what is needed for training the model (one month

As seen in Fig. 15, the daily average approximations of air change rates are in the acceptable range of their values in reality. According to the inspection and the survey, the apartment is being manually and randomly ventilated 13–24 h a day. For a personalized advice, the data in Fig. 15 can be compared to the standard daily recommended ACH value for the specific building. To investigate the validity of the results, the average monthly values found from Fig. 15 are compared to the wind velocity. The wind velocity is known to have a direct influence on the infiltration rate and on outdoor convective heat transfer coefficient. As seen in Table 10 and Fig. 16 (left), the higher wind velocities are associated with higher values of ACH. Furthermore, the CO_2 concentration values of the bedroom (where the highest peaks of CO_2 occur), show to be lower in the higher values of ACH, shown in Table 10 and Fig. 16 (right). This is an indication of the validity of the ACH approximations.

According to the building construction report, the average ventilation rate for this building is 1.84 ACH. The values found in Table 10 are in the same range of the assumed value and the average of the three months (1.53 ACH) leads to 3% deviation with the assumed average value, showing the reliability of the approximation. The values presented in Table 10 are depicted in Fig. 16.

Note that the accurate real values of ACH cannot be obtained since apart from the actual air-tightness of the building, the ventilation rate changes manually by the occupant. In addition to what is known as ventilation rate, random unknown factors such as the openings of the doors, ventilation grilles, and windows and the cleanness of the exhaust air channels can highly influence the ACH.

5. Conclusion

5.1. Conclusions

This study aimed to illustrate the extent to which it is possible to extract buildings' global thermo-physical characteristics, by measuring air temperature, and heating consumption data and feeding it to an inverse modelling problem of a simple 1R1C model.

From the entire process of measurement, collection, and handling the data and feeding it to the model, many important detailed practical lessons are learned. These are very important since in many pieces of research, the difference between computer-generated data and actual data and the consequent departures

are underestimated. In the actual circumstances, the occupants can apply significant levels of changes in many important variables such as ventilation rates and thermostat settings, resulting in a sys-

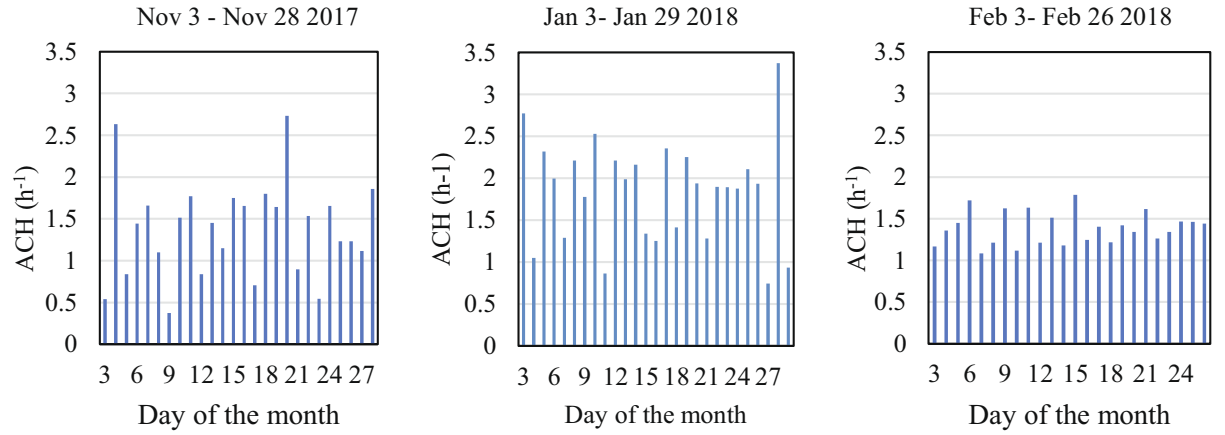

Fig. 15. Daily ACH rates obtained from the heat loss coefficient and the construction's thermal resistance.

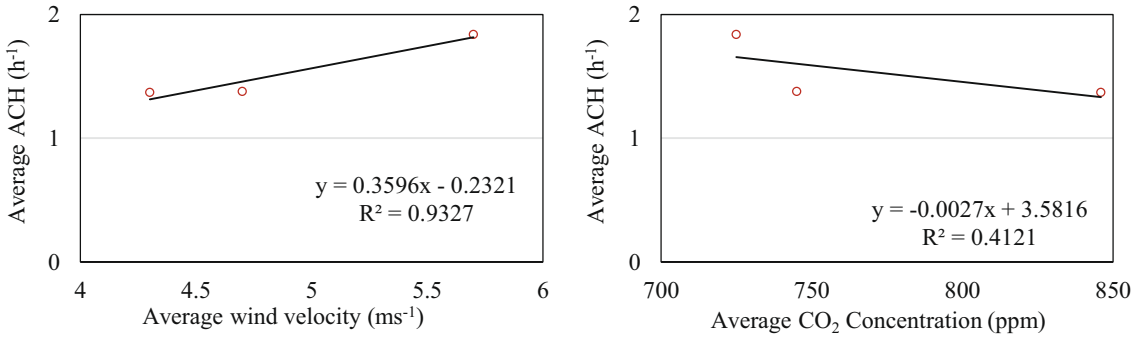

Fig. 16. The values and the trends of the monthly average of the daily ACH against average wind velocity (left) and average CO_2 concentration (right) showing a logical drift.

tem behavior that is difficult to mathematically model. The details for data filtering and cleaning are shared and explained. For filtering the data, the RH level in the bathroom has shown a critical role in the separation of the DHW and SH gas consumption from the smart meter readings. The air temperature also showed to help in filling the short-term heating consumption data gaps. The use of pattern recognition algorithms in combination with the applied method is recommended in the future studies.

During the optimization, unlike using heating demand for the RMSE function, by using temperature, the dynamic nature of the temperature history effect can be fully incorporated in the model. This is due to the fact that discretization methods can only cover a limited number of time steps before the present time. The optimization showed to work at its best during the winter period. This is suspected to be the consequence of the fact that the winter period contains heating data with a long range of values (e.g. large peaks), leading to a better training of the model. This limitation is no a barrier since the air heat losses are mainly critical in the winter, as a consequence of a need for enough air exchange while minimizing the heat losses.

The feed of data to the 1R1C model with different granularity levels has shown different results. This, for the solar gains and for the internal gains are due to the differences in hourly values and aggregated values. The dynamic effect of thermal mass shows to weaken as the granularity level increases. This is also in-line with the physics involved since by averaging the heating during a longer time period, the dynamic effects fade. Consequently, using hourly data, a better estimation of the global capacitance can be obtained. The estimation of the capacitance is expected to improve in houses with lower insulation, where the air temperature drifts are higher, improving the feed data to the model. The estimated heat loss coefficient showed very little differences when using different granularity level in the feed data. This is logical since a large part of this value is the transmission loss which is a static parameter. The differences in this value for different periods are due to the difference in different ventilation and infiltration rates. The range of this parameter, as well as the capacitance and solar fraction parameter is logical when evaluated with the construction data. After finding the four parameters, the heat loss coefficient was recalculated using the other three and the feed data, assuming the majority of changes to be associated with the changes in ventilation and infiltration losses. Using temperature data, losses can also be estimated. This however, requires the thermal transmittance of the building envelope, which can be found from the construction data and or preferably by making in-situ measurements. The values found with this approach have been validated using CO_2 concentration, average wind velocity, and the building's documented average air change rate. The expected trends and the values have shown a good agreement with the findings of the model, showing the reliability of the method and its outcomes.

In this case study, as expected, the year's coldest months have shown to result in the best fit in the optimization. This is a consequence of the large quantity of heating hours with large variations in the heating consumption data, resulting in better training of the model. Regarding the fact that the year of the measurements (2018) has had one of the hottest winters in the Netherlands, the shown performance of the method is expected to improve in other years when the cold period is longer and more extreme. It is important to note that the current study and the ones alike, by nature, do not lead to a high accuracy of parameter estimation as many parameters are lumped using assumptions. However, they serve other critical purposes such as comparative processes (e.g. choosing the candidate apartments for renovation in a block of many), general evaluation of buildings' performance with little effort and expense, and automated diagnosis of buildings' performance.

Table 10
Monthly average values of estimated ACH, average wind velocity, and average CO_2 concentration.

Parameter	November 2017	January 2018	February 2018
Average ACH (h^{-1})	1.37	1.84	1.38
Average Wind Velocity (ms^{-1})	4.3	5.7	4.7
Average CO_2 Concentration (ppm)	846	725	745

5.2. Recommendations for future studies:

As the outcomes for the solar radiation cannot be validated, this data should be measured on site, preferably per orientation, since the unknown local circumstances (e.g. a balcony extension on the top floor) can highly influence the solar gains. It is highly recommended to use orientation-specific solar radiation data for the input and to break down the solar gain term into different orientations in the equation to increase the accuracy of the predictions. For the present research, this data has not been available. Following the difference between actual and theoretical material properties, it is recommended to measure the in-situ thermal transmittance for the building envelope, following a standard method, during the data acquisition. This can lead to a higher accuracy when estimating air exchange rates. Along the same line, the data from the surface temperatures and heat fluxes can be used to feed a model of higher resolution to separate the construction's thermal resistance. Comparing the results of such model with the one used in this research is highly recommended. Furthermore, it is recommended to test the models by feeding the indoor air temperature of the living room and compare the results with the ones obtained based on the average air temperature. From a more gen-

eral perspective, it is recommended to explore a method to find the most important zone to measure its air temperature for the model.

CRediT authorship contribution statement

Arash Rasooli: Methodology, Software, Validation, Formal analysis, Investigation, Data curation, Writing - original draft, Writing - review & editing, Visualization, Project administration. **Laure Itard:** Conceptualization, Methodology, Validation, Investigation, Resources, Data curation, Writing - review & editing, Visualization, Supervision, Project administration, Funding acquisition.

Declaration of Competing Interest

The authors declare that they have no known competing financial interests or personal relationships that could have appeared to influence the work reported in this paper.

Acknowledgments

This project has been executed with help of “Topsector Energy Subsidy” of the Ministry of Economic Affairs and Climate Policy through OPSCHALER project. TKI iDEEGO and Rijksdienst voor Ondernemend Nederland (The Netherlands Enterprise Agency, RVO) are acknowledged.

References

[1] ISO, E. (2014), 9869: 1 Thermal insulation—Building elements—In-situ measurements of thermal resistance and thermal transmittance. International Organization for Standardization, Geneva.
[2] ISO, I. S. (2015). 9972: 2015 Thermal Performance of Buildings–Determination of Air Permeability of Buildings–Fan Pressurization Method. International Organization for Standardization: Geneva, Switzerland.
[3] Baker, P. (2011), Technical Paper 10: U-values and traditional buildings-In situ measurements and their comparisons to calculated values. technical report.
[4] I.A. Atsonios, I.D. Mandilaras, D.A. Kontogeorgos, M.A. Founti, A comparative assessment of the standardized methods for the in–situ measurement of the thermal resistance of building walls, Energy Build. 154 (2017) 198–206.
[5] A.-H. Deconinck, S. Roels, Comparison of characterisation methods determining the thermal resistance of building components from onsite measurements, Energy Build. 130 (2016) 309–320.
[6] K. Gaspar, M. Casals, M. Gangolells, A comparison of standardized calculation methods for in situ measurements of façades U-value, Energy Build. 130 (2016) 592–599.
[7] ASHRAE, H., 2001. ASHRAE fundamentals handbook. American Society of Heating Refrigeration and Air- Conditioning Engineers. Atlanta GA.
[8] L. Raillon, Experimental Identification of Physical Thermal Models for Demand Response and Performance Evaluation, Doctoral dissertation, Saint Gobain, France, 2018.
[9] R. Ricciu, F. Ragnedda, A. Galatioto, S. Gana, L.A. Besalduch, A. Frattolillo, Thermal properties of building walls: indirect estimation using the inverse method with a harmonic approach, Energy Build. 187 (2019) 257–268.
[10] K. Chaffar, A. Chauchois, D. Defer, L. Zalewski, Thermal characterization of homogeneous walls using inverse method, Energy Build. 78 (2014) 248–255.
[11] A. Rasooli, L. Itard, In-situ rapid determination of walls' thermal conductivity, volumetric heat capacity, and thermal resistance, using response factors, Appl. Energy 253 (2019) 113539.
[12] T. Šuklje, M. Hamdy, C. Arkar, J.L. Hensen, S. Medved, An inverse modeling approach for the thermal response modeling of green façades, Appl. Energy 235 (2019) 1447–1456.
[13] A.-H. Deconinck, S. Roels, The as-built thermal quality of building components: characterising non-stationary phenomena through inverse modelling, Energy Procedia 132 (2017) 351–356.
[14] L. Evangelisti, C. Guattari, P. Gori, F. Asdrubali, Assessment of equivalent thermal properties of multilayer building walls coupling simulations and experimental measurements, Build. Environ. 127 (2018) 77–85.
[15] Y.M. Lee, L. An, F. Liu, R. Horesh, Y.T. Chae, R. Zhang, Applying science and mathematics to big data for smarter buildings: Smarter buildings, Ann. N.Y. Acad. Sci. 1295 (1) (2013) 18–25.
[16] P. Bacher, H. Madsen, Identifying suitable models for the heat dynamics of buildings, Energy Build. 43 (7) (2011) 1511–1522.
[17] Rasooli, A., Itard, L., Meijer, A., 2017. Energy and Comfort Monitoring in Existing Buildings: A LargeScale Measurement Campaign of 150 Dutch Dwellings, in ASHRAE 6th International Conference: ENERGY in BUILDINGS 2017, ASHRAE: Athens, Greece.
[18] Costola, D., Melo, A.P., Jacob, L., 2017. Development of Energy Simulation Models from Smart Meter Data using Inverse Modelling and Genetic Algorithms. Proceedings of the 15th IBPSA ConferenceSan Francisco, CA, USA, Aug. 7-9, 2017.
[19] R. Kramer, J. van Schijndel, H. Schellen, Inverse modeling of simplified hygrothermal building models to predict and characterize indoor climates, Build. Environ. 68 (2013) 87–99.
[20] Y. Zhang, Z. O'Neill, B. Dong, G. Augenbroe, Comparisons of inverse modeling approaches for predicting building energy performance, Build. Environ. 86 (2015) 177–190.
[21] B. Dong, C. Cao, S.E. Lee, Applying support vector machines to predict building energy consumption in tropical region, Energy Build. 37 (5) (2005) 545–553.
[22] S. Karatasou, M. Santamouris, V. Geros, Modeling and predicting building's energy use with artificial neural networks: methods and results, Energy Build. 38 (8) (2006) 949–958.
[23] An, L., Chae, Y.T., Horesh, R., Lee, Y., Zhang, R., 2013, December. An inverse PDE-ODE model for studying building energy demand. In 2013 Winter Simulations Conference (WSC) (pp. 1869-1880). IEEE.
[24] González-Vidal, A., Ramallo-González, A. P., Terroso-Sáenz, F., & Skarmeta, A. (2017, December). Data driven modeling for energy consumption prediction in smart buildings. In 2017 IEEE International Conference on Big Data (Big Data) (pp. 4562-4569). IEEE.
[25] K.P. Lam, J. Zhao, E.B. Ydstie, J. Wirick, M. Qi, J.H. Park, An EnergyPlus whole building energy model calibration method for office buildings using occupant behavior data mining and empirical data, ASHRAE J. (2014) 160–167.
[26] J.E. Braun, N. Chaturvedi, An inverse gray-box model for transient building load prediction, HVAC&R Res. 8 (1) (2002) 73–99.
[27] V. Gori, C.A. Elwell, Estimation of thermophysical properties from in-situ measurements in all seasons: Quantifying and reducing errors using dynamic grey-box methods, Energy Build. 167 (2018) 290–300.
[28] G. Nordström, H. Johnsson, S. Lidelöw, Using the energy signature method to estimate the effective U-value of buildings, in: Sustainability in Energy and Buildings, Springer, Berlin, Heidelberg, 2013, pp. 35–44.
[29] M. Senave, S. Roels, G. Reynders, S. Verbeke, D. Saelens, Assessment of data analysis methods to identify the heat loss coefficient from on-board monitoring data, Energy Build. 209 (2020) 109706, https://doi.org/10.1016/j.enbuild.2019.109706.
[30] C. Ghiaus, Experimental estimation of building energy performance by robust regression, Energy Build. 38 (6) (2006) 582–587.
[31] M. Senave, G. Reynders, P. Bacher, S. Roels, S. Verbeke, D. Saelens, Towards the characterization of the heat loss coefficient via on-board monitoring: Physical interpretation of ARX model coefficients, Energy Build. 195 (2019) 180–194.
[32] Senave, M., Roels, S., Verbeke, S., Lambie, E., Saelens, D., 2019. Sensitivity of characterizing the heat loss coefficient through on-board monitoring: A case study analysis. Energies, 12(17), 3322.
[33] D. Farmer, D. Johnston, D. Miles-Shenton, Obtaining the heat loss coefficient of a dwelling using its heating system (integrated coheating), Energy Build. 117 (2016) 1–10.
[34] Bauwens, G., 2015, In Situ Testing of a Building's Overall Heat Loss Coefficient-Embedding Quasi-stationary and Dynamic Tests in a Building Physical and Statistical Framework, PhD thesis, KU Leuven, Belgium.
[35] S. Roels, P. Bacher, G. Bauwens, S. Castaño, M.J. Jiménez, H. Madsen, On site characterisation of the overall heat loss coefficient: Comparison of different assessment methods by a blind validation exercise on a round robin test box, Energy Build. 153 (2017) 179–189.
[36] Annex 71 (2017), IEA EBC Annex 71: building energy performance assessment based on in situ measurements.
[37] Pandraud, G., Mangematin, E., Roux, D., Quentin, E., 2013. QUB: a new rapid building energy diagnosis method. In Proceedings of CLIMA 2013.
[38] Sougkakis, V., Meulemans, J., Alzetto, F., Wood, C., Gillott, M., Cox, T., 2017, September. An assessment of the QUB method for predicting the whole building thermal performance under actual operating conditions. International SEEDS Conference 2017: Sustainable Ecological EngineeringDesign for Society, Leeds Beckett University, Leeds, United Kingdom. ffhal-01589204.
[39] Ahmad, N., Ghiaus, C., Thiery, T., 2020. Influence of Initial and Boundary Conditions on the Accuracy of the QUB Method to Determine the Overall Heat Loss Coefficient of a Building. Energies, 13(1), 284.
[40] Boisson, P., Bouchié, R., 2014. ISABELE method: In-situ assessment of the building envelope performances. in 9th International Conference on System Simulation in Buildings.
[41] R. Kramer, J. Van Schijndel, H. Schellen, Simplified thermal and hygric building models: a literature review, Front. Architectural Res. 1 (4) (2012) 318–325.
[42] Andrade-Cabrera, C., De Rosa, M., Kathirgamanathan, A., Kapetanakis, D.S., Finn, D., 2018, May. A Study on the Trade-off between Energy Forecasting Accuracy and Computational Complexity in Lumped Parameter Building Energy Models. In The 10th Canada conference of International Building Performance Simulation Association (eSim 2018), Montreal, Canada, 9-10 May 2018. IBPSA.
[43] T. Berthou, P. Stabat, R. Salvazet, D. Marchio, Development and validation of a gray box model to predict thermal behavior of occupied office buildings, Energy Build. 74 (2014) 91–100.
[44] I. Hazyuk, C. Ghiaus, D. Penhouet, Optimal temperature control of intermittently heated buildings using Model Predictive Control: Part I – Building modeling, Build. Environ. 51 (2012) 379–387.

[45] M. Trčka, J.L. Hensen, Overview of HVAC system simulation, Autom. Constr. 19 (2) (2010) 93–99.
[46] An, L., Chae, Y. T., Horesh, R., Lee, Y. M., Reddy, C.K., 2013. U.S. Patent No. 8,620,632. Washington DC, USA.
[47] Park, H., Ruellan, M., Bouvet, A., Monmasson, E., Bennacer, R., 2011, Octobe. Thermal parameter identification of simplified building model with electric appliance. In 11th International Conference on Electrical Power Quality and Utilisation (1-6). IEEE.
[48] H. Park, N. Martaj, M. Ruellan, R. Bennacer, E. Monmasson, Modeling of a building system and its parameter identification, J. Electr. Eng. Technol. 8 (5) (2013) 975–983.
[49] M. Zeifman, A. Lazrak, K. Roth, Residential retrofits at scale: opportunity identification, saving estimation, and personalized messaging based on communicating thermostat data, Energ. Effi. 13 (3) (2020) 393–405.
[50] A.P. Ramallo-González, M. Brown, E. Gabe-Thomas, T. Lovett, D.A. Coley, The reliability of inverse modelling for the wide scale characterization of the thermal properties of buildings, J. Build. Perform. Simul. 11 (1) (2018) 65–83.
[51] S. Wang, X. Xu, Parameter estimation of internal thermal mass of building dynamic models using genetic algorithm, Energy Convers. Manage. 47 (13-14) (2006) 1927–1941.
[52] Mihail–Bogdan, C.Ă.R.U.Ț.A.Ș.I.U., Constantin, I.O.N.E.S.C.U., Horia, N.E.C.U.L.A., 2016. The influence of Genetic Algorithm parameters over the efficiency of the energy consumption estimation in a low– energy building. Energy Procedia, 85, 99-108.
[53] Gupta, P., 2017. Inverse Modelling for Determination of Resistance & Capacitance of Typical Dutch Residences Using Genetic Algorithms, MSc thesis, Electrical Engineering, Mathematics and Computer Science. 2017, Delft University of Technology, Netherlands.
[54] Van Schijndel, J., Uittenbosch, S., 2011. Determination of Hygrothermal Properties for Building Materials using Inverse Modeling Techniques. in 9th Nordic Symposium on Building Physics-NSB 2011, Tampere, Finland, 29 May-2 June, 2011.
[55] Ioannou, A., 2018. Thermal comfort and energy related occupancy behavior in Dutch residential dwellings. A+ BE| Architecture and the Built Environment, (27), 242-242., PhD Thesis, Delft University of technology, the Netherlands.
[56] (KNMI), K.N.M.I. The Royal Netherlands Meteorological Institute. Available from: https://www.knmi.nl/over- het-knmi/about.
[57] S. Royer, S. Thil, T. Talbert, M. Polit, A procedure for modeling buildings and their thermal zones using co-simulation and system identification, Energy Build. 78 (2014) 231–237.